Influence of fibre orientation, moisture absorption and repairing performance on the low-velocity impact response of woven flax/Elium® thermoplastic bio-composites

R Manaii[1,2], S Terekhina[1], L Chandreshah[3], N Shafiq[3], D Duriatti[2] and L Guillaumat[1]

Abstract

The importance of natural reinforced bio-composite materials with desirable properties such as high modulus-to-weight ratio, good impact resistance, and the ability to be easily repaired is crucial in the industry. A woven flax/Elium® thermoplastic bio-composite is manufactured to challenge these needs. Elium® is the only resin that permits the manufacture of large parts with thermoset-like processes, as Liquid Resin Infusion presented in that work. The paper highlights the influence of stacking fibre orientation, moisture absorption, and repair aptitude on its impact resistance. An instrumented drop tower was needed to conduct low-velocity impact tests at several energies and high-speed image coupled with microscopic observations was used to assess the damage evolution. The impact resistance was improved for the dry $(0/90)_6$ orientation, but moisture absorption decreased its impact peak force by 20%. A three-point bending test was preferred to compression after impact for studying the residual properties after impact. The bio-composites with $(\pm45)_6$ orientation showed higher impact residual performance than the $(0/90)_6$ orientation, and corresponded to the reduction of maximum bending force by 20% than that of the reference. In addition, a thermo-compression process was applied to repair the impacted plates and conduct multiple impact/repair cycles which showed a significant recovery of stiffness and maximum impact force at 4J on $(0/90)_6$ plates, highlighting their potential for repair in the automotive and marine industries.

Keywords

Woven bio-composites, flax fibre, thermoplastic acrylic-based Elium®, low-velocity impact, repair damage, hygrothermal ageing

Highlights

- Impact behaviour of the woven flax/Elium® thermoplastic bio-composites is highlighted
- Influence of stacking orientation, moisture uptake and repair aptitude is studied
- Impact resistance for the dry $(0/90)_6$ orientation is improved
- Best impact residual performance for $(\pm45)_6$ orientation
- Interesting potential to repair is observed.

Introduction

The extensive usage of fibre reinforced polymer matrix composites has paved the way to produce novel combinations of materials for various applications, such as shipping, aerospace, automobile. Various fibres (synthetic or natural) and matrices (thermoset or thermoplastic) have been experimented with for manufacturing these composites. Among them, thermoplastic (TP) composites have gathered significant attention due to their recyclability, rapid manufacturing, thermo-formation and damage repair, higher modulus-to-weight ratio and

[1]Laboratoire Angevin de Mécanique, Procédés et innovAtion, Arts et Métiers Institute of Technology, Angers, France
[2]Group Depestele, Research and Development, Bourguebus, France
[3]Civil Engineering lab, UTP, Seri Iskandar, Malaysia

Corresponding author:
S Terekhina, Laboratoire Angevin de Mécanique, Procédés et innovAtion, Arts et Métiers Institute of Technology, 2 Bd du Ronceray, Angers 49035, France.
Email: svetlana.terekhina@ensam.eu

impact absorbing.[1–3] However, the higher viscosity of the thermoplastic resin in the molten state can impair fibre impregnation, which consequently limits their use in Liquid Resin processes that are still common for thermoset applications (as for boat hull, aircraft fuselage…). In addition, the TP matrices are available in film or pellet forms and require high-temperature processing and costly equipment, like autoclave and hot press.[3,4] Therefore, there is an increasing demand for a thermoplastic resin that can be processed at room temperature and provides outstanding impact and mechanical properties. The liquid thermoplastic acrylic-based Elium® by Arkema overcomes this problem. Nowadays, it is the only resin that permits the manufacture of large parts using thermoset-like processes at room temperature, such as pultrusion, Bladder Assisted Resin Transfer Molding, or Liquid Resin Infusion (LRI).[5–7] However, to ensure the long-term structural safety and durability of composite structures, materials with high impact resistance are necessary to minimize the degradation caused by impacts during their service life. The damage may be caused, for examples, by the dropping of the tool while in maintenance, bird strike, runway debris hitting, etc. So, impact damage is a serious challenge as it significantly degrades the structural integrity of the composite and sometimes generates not visible to the naked eye damage.[8] The latter is one of the major obstacles to its maintenance.[9] During the low-velocity impact test, the different damage mechanisms affect the structure internally like delamination at the interface between layers, matrix cracking, fibre/matrix debonding, and fibre breakage.[10,11] Therefore, various approaches have been exploited to improve the impact resistance and damage tolerance of composite. They include the choice of fabric architecture,[10] the toughening of thermosetting resin by adding the nano-particles,[12,13] or the use of z-fibre pinning to avoid delamination.[14] Despite their abundant use, unidirectional composites (UD) exhibit poor resistance under transverse loadings involving delamination, matrix damage, and fibre failure.[8,15] The woven composites based on the polymeric resin are assumed to improve impact energy absorption[10] and inter-laminar fracture toughness, resulting in greater resistance to delamination[16] when compared to unidirectional (UD) laminated composites. It is necessary to note that the acrylic TP Elium® based composite has shown better damage energy absorption capacity compared to the epoxy-based one.[6,17] Already the processing,[5–7,18] vibration damping,[19] the fracture toughness (Mode I),[20,21] and mechanical properties[22,23] attributes of the composite system manufactured with this resin are investigated in detail. However, above mentioned researches concern usually, the Elium® based composites reinforced by synthetic fibres (glass or carbon).[6,7,24] Nevertheless, given the issues of global warming, high energy consumption, and pollution associated with synthetic composites derived from petroleum products, there is an urgent need to investigate the impact properties of natural fibre/Elium® composites. Natural fibres have some interesting characteristics. They are cost-effective, renewable, available in high quantity, have low fossil-fuel energy requirements, and can offer good physical and mechanical properties (low density, good specific mechanical properties, vibrational damping, and impact absorbing).[25,26] They are now considered a serious alternative to glass fibres for reinforcement in polymer matrix composites.[27,28] Composites based on plant fibres are used in automotive parts (car bumpers, doors, space for a spare wheel and sports car rear wing, front and rear aprons, front spoiler, front, and rear lids as well as the mudguards and diffuser) to reduce the mass of components and decrease production energy consumption by 80%.[1] Therefore, the combining beneficial properties of each constituent make the use of flax/Elium® composites attractive, highlighting their potential for different widespread applications, especially in automotive and marine industries. The additional advantage of these composites is their post-thermoformability which offers new material assembling possibilities.[5,29]

The damage caused by a low-velocity impact can be repaired by different methods such as patch, bolted and bonded repairs, fusion repair, or post-thermoformability.[2,5,11] The latter is interesting thanks to the fusion capacity of thermoplastic resin. It is enough to apply heat and pressure for repairing the damaged region. Reyes and al. Show that the 4-point bending test of the repair after low-velocity impact at 16J by simple compression molding samples reveals a significant recovery in the flexural strength and modulus of the thermoplastic woven glass/PP composites.[11] This is available for both considered fibre volume configurations of 50/50 and 20/80 in the warp and fill directions. He also underlines that the maximum recovery of post-impact residual properties is limited by fibre breakage damage.

The impact resistance of bio-composites is also affected by extreme environmental conditions, such as temperature, humidity, or hygrothermal ageing. Moisture absorption is one of the very important issues that need to be resolved to achieve better performance of plant fibres and their composites since they can absorb more water than synthetic fibre composites.[30] The authors conducted a literature review to examine the influence of hygrothermal ageing on the impact properties of the composites and found that the damaged area of aged samples increased under low-velocity impact, resulting in decreased post-impact performance.[31,32]

It is clear that further studies are necessary for the development of eco-friendly composites based on the Elium® matrix for their effective use in structural applications. Furthermore, the quantification of the residual

strength after impact and the investigation of damage repair is paramount for the successful use of thermoplastic composite materials.

Current research is focused on investigating the impact benefits offered by the novel room temperature cure reactive liquid Methyl-methacrylate (MMA), Elium® thermoplastic resin composite reinforced by woven flax fibres. The paper highlights the influence of stacking fibre orientation, moisture absorption and repair aptitude on its low-velocity impact resistance.

Material and manufacturing process

Material properties

The bio-composite used in the study composes of the thermoplastic Elium®188 resin, recently formulated by Arkema (France), and the flax 2/2 twill weave fabric (Figure 1(a)) produced and provided by Depestele company (France). The fabric weight is 360 g/cm^2. The physical and mechanical properties of the studied bio-composite, as also its constituents are given in Table 1.

One big challenge of the flax fibres is that they are hygroscopic, which means that they readily absorb moisture from their surroundings. To overcome this problem, the drying of the fibres before the infusion process was carried out at 60°C in a vacuum oven for 6 h. This time is required to stabilize the weight loss of the fibre.

Woven twill flax/Elium® plates compose of six layers. Two stacking sequences for dry condition were considered: $(0/90)_6$ and $(\pm 45)_6$.

Since the flax fibres are sensitive to moisture uptake, the samples with stacking orientation $(0/90)_6$ were exposed to hygrothermal ageing in a climatic chamber (EXCAL 2211-HA, France), as recommended by ISO62 (2008-05-01) standard,[34] before the impact tests to assess the effect of moisture on their impact performance. The latter was aged at 70°C and 75% of relative humidity for about 2 months to follow an complete evolution of the mass uptake (Figure 1(b)). However, only the samples with maximum moisture uptake were considered for the impact tests and referenced as *75%RH_090*. The choice of that woven fibre stacking orientation is motivated by its supposed better impact resistance (higher contact stiffness) than in the case of $(\pm 45)_6$ one, and therefore, the influence of material properties (moisture uptake of flax fibres) on its impact performance.

The mass gain of aged samples is expressed in % by:

$$M_t = \frac{m_t - m_0}{m_0} \cdot 100 \quad (1)$$

where $\mathbf{m_0}$ and $\mathbf{m_t}$ are the masses of samples measured before ageing and at instant $\boldsymbol{t}$ of ageing respectively.

Results of hygrothermal condition show that the maximum moisture uptake (1.57±0.17%) is reached after around 10 h$^{1/2}$, followed by its decreasing, which means the bio-composite is losing mass probably due to a hydrolysis process (Figure 1(b)).

Manufacturing process

Liquid resin infusion. Composite plates of dimensions $1000 \times 750\, mm^2$ and a thickness in the range of 4.5–4.8 mm were manufactured using the Liquid Resin Infusion (LRI) process by CMP company (France) under a vacuum pressure of −0.95 bar (−95 kPa) at room temperature. The process consists of preparing first the glass mold with a release agent, then depositing of dry fibres with the desired stacking sequence, followed by a peel ply as well as an infusion complex composed of a micro-perforated film and an infusion mesh to facilitate the resin migration. Finally, an impermeable film was attached to the mold with an adhesive sealer. This vacuum bag contains a resin inlet initially closed and an outlet connected to the vacuum pump. The resin has been degassed

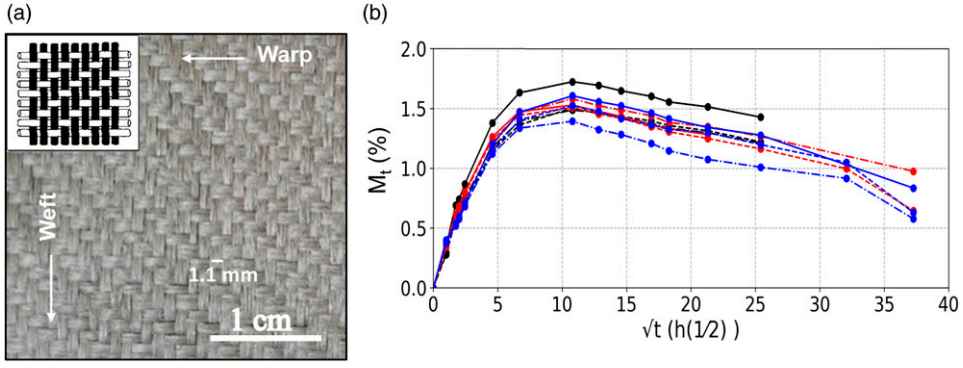

Figure 1. (a) Flax twill fabrics from Depestele, (b) Evolution of the mass uptake during hygrothermal ageing: black, red and blue color points represent three batches composed of three samples tested during the hygrothermal ageing.

Table 1. Physical and mechanical properties of the bio-composites considered in the present work.

Properties	Elium®188[29]	Flax fibres[33]	Flax fabric	Woven flax/Elium® composite		Standard
				$(0/90)_6$	$(\pm45)_6$	
Density (kg/m^3)	1.19	1.45	—	1.2 ± 0.02		ISO 527
Surface density (g/cm^2)	—	—	360	—		
Viscosity (mPa.s) at 25°C	100	—	—	—		
Tensile modulus (GPa)	3.2	12-85	—	11.5 ± 0.4	3.6 ± 0.1	
Ultimate tensile stress (MPa)	66	600-2000	—	110 ± 4	55 ± 4	
Elongation at break, **A** (%)	2.8	1–4	—	1.6 ± 0.15	15.3 ± 1.25	

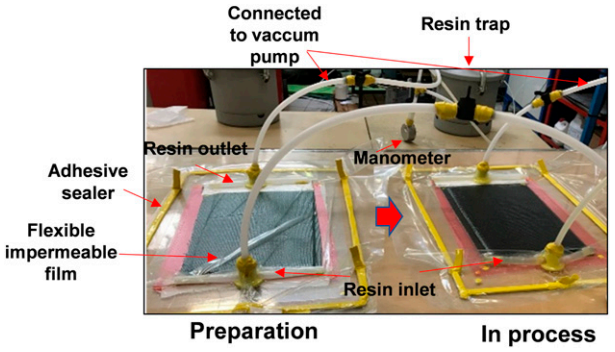

Figure 2. Preparation of the components and infusion process.

before infusion for better specimen quality. The summary view of this process is shown in Figure 2.

The fibre volume fraction V_f of obtained samples was corresponded to 39%.

Thermo-compression process. A thermo-compression process was used to repair the impacted plates with the following methodology:

- Setting up the temperature of the press to 200°C to attend to the melting temperature of Elium®;
- Applying the pressure of 5.5 kPa for 5 min;
- Cooling with natural convection to room temperature (about 2 h).

Measurement and characterization

Methodology description

First, the woven twill flax/Elium® composites with stacking orientation of $(0/90)_6$ and $(\pm45)_6$ will be subjected to impact energies between 7 and 22 J using an instrumented dropping weight impact tower. Second, dry and aged impacted samples of that composite with $(0/90)_6$ stacking orientation will be compared at the considered applied impact energies. Finally, the possibility of damage repair after impact of $(0/90)_6$ flax/Elium® composites will be investigated using a thermo-compression process. The repair samples will be subjected to multiple impact/repair tests at impact energies of 4 and 7 J to evaluate their stiffness and maximum impact force recovery. In addition, the impacted and undamaged dry $(0/90)_6$ and $(\pm45)_6$ flax/Elium® composites will be tested under 3-point bending loading conditions to evaluate the effect of impact energy on residual flexural properties.

Low velocity impact (LVI) tests

The low-velocity impact tests were performed with the in-house drop weight impact tower (Figure 3(a)). The setup consists of the dropping carriage with an impactor sliding on the guide rails and two fixed metallic supports with the clamping system of the sample shown in Figure 3(a). The principle is to fall free the dropping mass and impact the sample at the centre in three-point bending configuration. The impactor used for the impact tests is hemispherical in shape with a diameter of *16 mm,* as recommended by the Airbus standard AITM 1-0010.[35] The total mass, including carriage and impactor is approximately equal 1 kg. Two laser and piezoelectric sensors were used for measuring the displacement of the impactor and sample deflection, and the load respectively, during the impact. The laser sensor for monitoring the sample deflection is located underneath it and pointed at its centre.

Impact samples of dimensions $100 \times 150 \times 4.5\,mm^3$ have been cut from the plates of dimensions $1000 \times 750\,mm^2$ according to Airbus standard AITM 1-0010.[35] All the specimens were then stored in the dry atmosphere of a desiccator prior to testing. The ambient conditions during tests were 23°C and 50% RH.

LVI parameters. The impact velocity is determined from the experimental curve of the impactor's displacement versus test duration and corresponded to its slope. The latter is compared with the theoretical one, estimated by equation (2):

$$V_{th} = \sqrt{2gh} \quad (2)$$

Table 2 summarizes the impact test conditions for the considered bio-composites. Table 2 shows a relative deviation of about 10–15% between the true and theoretical values of impact velocity due to the test conditions: wear between the dropping carriage and the guide rails, wear of the air, etc. We made the choice to consider the theretical heights and measure the real velocities. Note, the choice of 4J and 7.5J of impacted energy for the repair samples is justified by generation or not the fibre breakage after the impact.

For each considered condition, the tests were repeated three times for validation to ensure test repeatability.

In the present study, the improvement of the impact property will be quantified in terms of the maximum load peak and the deflection corresponding to the maximum load increase, but also it will be evaluated in terms of absorbed energy and the contact duration. During the impact, the energy is decomposed into two parts: *an absorbed energy* and *an elastic energy*[36,37] (Equation (3)) (Figure 3(b)). *Elastic energy* ($E_{elastic}$), can be defined as the amount of energy recovered after impact and *absorbed energy* ($E_{absorbed}$) as the difference between incident impact and elastic energies. Also, the area under the force-deflection curve gives the amount of energy that has been absorbed by the system: sample, impactor, and boundary conditions[26] (Figure 3(b)). This energy shows the part of the impact energy that was not returned to the impactor (case without perforation of the sample). The absorbed energy can also be simply estimated from equation (4).[37] Both integration of force-displacement impact curves and equation (4) are considered in this study.

$$E_{impact} = E_{absorbed} + E_{elastic} \quad (3)$$

$$E_{absorbed} = \frac{1}{2} m \left(V_i^2 - V_r^2 \right) \quad (4)$$

where m is the impactor mass (kg), V_i and V_r are impact and rebond velocities respectively, (m/s).

The temporal evolution of the contact force during an impact could be described by the relationship derived from a

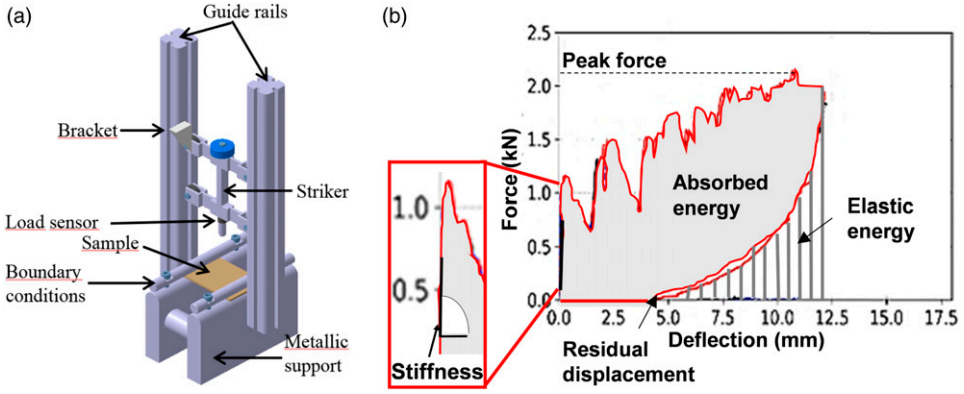

Figure 3. (a) Drop weight tower; (b) Schematic view of the definition of impact energy.

Table 2. Impact test conditions for the considered bio-composites.

Test condition	Orientation	Height (m)	Theoretical impact velocity (m/s), equation (2)	Impact velocity (m/s)	Impact energy (J), equation (3)	Standard deviation
dry	$(0/90)_6$	1	4.43	3.89	7.5	0.36
		2	6.26	5.0	12.5	1.40
		3	7.67	6.54	21.4	1.50
Aged	$(0/90)_6$	1	4.43	3.87	7.5	0.36
		2	6.26	4.98	12.43	1.40
		3	7.67	6.5	21.1	1.50
Repaired	$(0/90)_6$	0.5	3.13	2.82	4.0	0.2
		1	4.43	3.87	7.5	0.36
Dry	$(\pm 45)_6$	1	4.43	4.2	8.5	0.7
		2	6.26	5.75	15.5	1.45
		3	7.67	6.86	22.77	1.80

mass-spring vibration system, proposed by Schoeppner and Abrate.[38]

$$F(t) = V\sqrt{Km}\sin\left(\sqrt{Kt/m}\right) \quad (5)$$

$$t_{contact} = \frac{\pi}{\sqrt{K/m}} \quad (6)$$

The relationships (Equations (5) and (6)) show the stiffness structure and the impactor mass affects the contact time. Since the latter was not varied throughout the tests, only the stiffness could change and decreases as the contact time increased.

The variables of equations (5) and (6) are: - *F: Force, V: Velocity, t: Time, K: stiffness constant, and m: Impactor Mass.*

Post-impact bending

The Airbus standard AITM1-0010 recommends realizing compression after impact (CAI) tests to measure the residual resistance of impacted specimens.[35,39] The CAI is a suitable test when the impact induces delamination. The latter has a significant effect (opening mode) during the compression test if the sample length is situated in the load direction. However, since the matrix of the present biocomposite is thermoplastic, few delamination was observed. Therefore, another mechanical loading is needed to evaluate a better relevant post-impact performance. Accordingly, we have chosen to do a three-point non-standardized bending test that most closely resembles the impact configuration. The crosshead speed was 1 mm/min. The test continues until 75% of the maximum force supported by the sample. This is necessary to prevent the sample from moving away at the end of the test. The tests were performed on a 100 kN universal testing machine, and the diameter of metallic supports is the same as for the ones of low-velocity impact.

Damage characterization

Optical observation. The post-mortem damage mechanisms of the impacted samples were observed using an optical microscope Zeiss Axio Imager M2m (Germany). Before, the samples were molded in epoxy resin and polished.

High-speed camera observation. As the contact duration of the impactor/sample is around 10 ms, the use of a high-speed camera is necessary. It allows us to analyze the local instability phenomena during the impact, but also observe the visual deflection profile of the sample. For comparison reasons, the camera was set up at different angles to obtain cross-reference images.

Profilometry. The Bruker optic profilometer was used to measure the indentation depth after impact and the surface damage profile. The aim is to quantify the impact damages being subjected to by the samples.

Results and discussions

Impact response depending on the stacking orientation

Impact load influence. The force versus impact duration at different energy levels for both considered composites with stacking orientation ($(0/90)_6$ and $(\pm45)_6$) is illustrated in Figure 4. The curves show significant oscillations, which are generally due to vibrations of the system elements (samples, impactor, and boundary conditions). Note that the shock can be assimilated to a temporal dirac which corresponds to a frequency white noise which activates many frequency eigenmodes.[38]

In general, the curves show an increase in the contact force up to a maximum value and then decrease until its cancellation, which indicates the loss of contact between the impactor and the sample. In the present study, a first peak, corresponding to a first drop in the force, is observed very early, around 1 ms. This phenomenon has often been linked to a very local interaction between the impactor and the sample due to the nature of the material, and mainly its stiffness.[7,40] Figure 4(a)–(d) also shows that the maximum force increases with the impact energy (in the range of 7-22J) and this is for whatever stacking orientation. It is also possible to see that the maximum force is similar for the two considered orientations as this was not expected. It could be explained by both stiffness and damage influence on the impact properties. In the case of $(0/90)_6$ orientation, the stiffness of the sample is twice higher that for the $(\pm45)_6$ one, due to the orientation of fibres in the axis of the bending load, which principally supported the impact. However, its crack, and therefore, damage propagation is faster than in the orientation $(\pm45)_6$ due to the bending effect provided by the clamped system (Figure 4(e)). For the latter, the cracking is mainly oriented at 45° corresponding to the direction of fibres that are not orientated in the bending axis, and governed by shear phenomenon between the fibres (Figure 4(f)). Note that the contact time increases with the applied energy, which depends slightly on the stacking orientation. It is greater for the $(\pm45)_6$ than for the $(0/90)_6$ of about 22% and 10% for 12J and 22J impact energies, and varies from 6 to 10 ms for the $(\pm45)_6$. Therefore, the more the incident energy increases, the more the damage develops, which implies a reduction in the stiffness and consequently, an increase in the contact time.

Deflection after impact. The deflection curves versus impact time duration, measured at the centre of the back face

sample, are given in Figure 5. Note that the fluctuations on the curves at 22 J corresponding to $(\pm 45)_6$ orientation are due to noticeable local damage induced on the back surface (see Figure 8(h)). Figure 5 shows the temporal evolution of deflection that is not symmetrical. The curve does not return to zero when the impactor leaves the sample and subsequently when the contact force is canceled.

A permanent deformation after impact is therefore observed that could be explained by the nature of both thermoplastic matrix and flax fibres. This is also confirmed by the fact that it increases with the impact energy, varying from 1 to 6 mm. The permanent deflection depends also on the choice of fibre orientation. It can be observed that the samples with $(\pm 45)_6$ have a much higher permanent deflection value (corresponding to 48.5% and

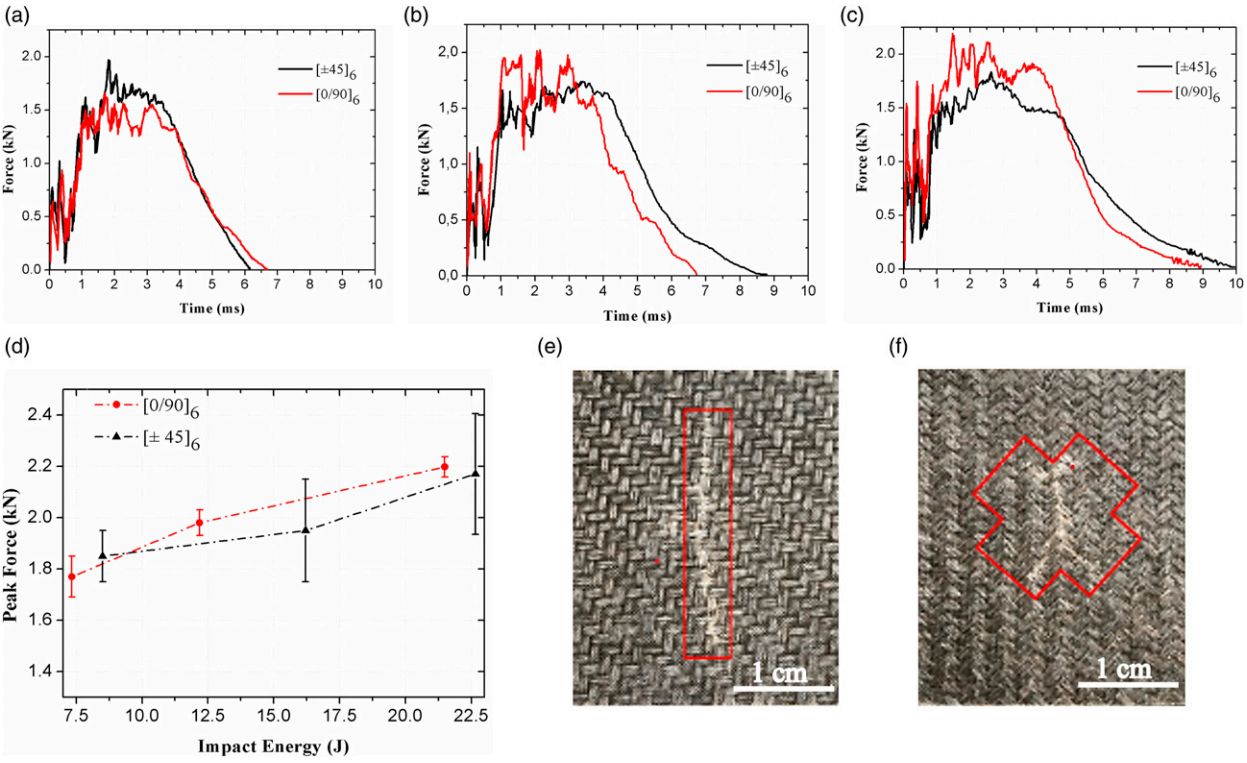

Figure 4. Load versus impact time for around: (a) 7 J, (b) 12 J, (c) 22J, (d) Peak force evolution versus impact energy. Back face of damaged flax/Elium® bio-composites impacted at 12 (j) (e) $(0/90)_6$ (f) $(\pm 45)_6$.

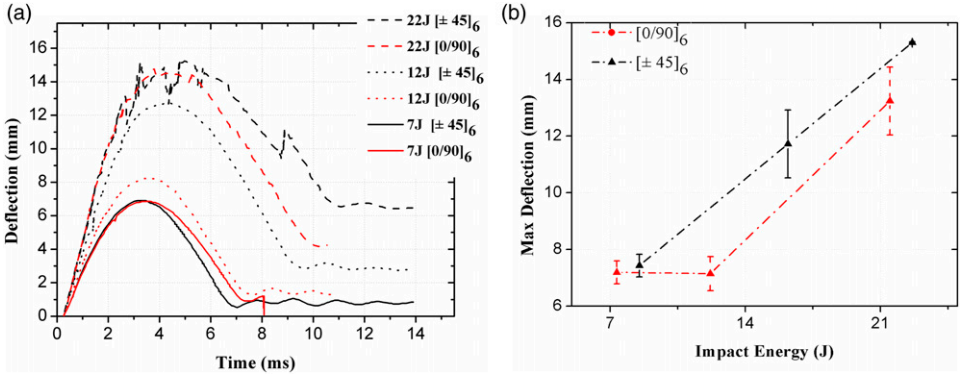

Figure 5. (a) Deflection versus impact time for around 7 J, 12 J and 22J, (b) max deflection evolution versus impact energy for $(0/90)_6$ and $(\pm 45)_6$ orientations.

35% at 12J and 22J respectively) than the $(0/90)_6$ ones for energies higher than 8 J, as shown in Table 3.

Indeed, the samples with $(\pm45)_6$ fibre orientation will promote the role of the thermoplastic matrix and the fibre/matrix interface cohesion, whereas the $(0/90)_6$ samples ensure the structure thanks to the fibres orientated at 0°. A similar trend is observed for the evolution of the maximum deflection as the applied impact energy increases (Figure 5(d)) and the stacking orientation changes from 0° to 45°. It is also confirmed by a good agreement with the measurements by profilometry of the impacted depth (Figure 6). Note that Figure 6 shows the scans with many oscillations due to the surface condition of the samples, which are rough and not perfectly flat. It is more pronounced with increasing impact energy, and therefore damage evolution. Once again, the indentation after impact is deeper for $(\pm45)_6$ samples than for $(0/90)_6$ ones at impact energies higher than 8J. It corresponds to 71% for the samples $(\pm45)_6$ at 22J. Therefore, the samples with stacking orientation $(0/90)_6$ present a better impact resistance in comparison with $(\pm45)_6$ one for the three considered energy levels.

Absorbed energy effect after impact. The force-deflection curves at 7J, 12J, and 22J are presented in Figure 7 for both dry-considered stacking orientations. During the impact, the kinetic energy of the impactor is transferred to the plate and dissipated through the various damage mechanisms. It can be seen that during the eventual rebound phase, not all the energy transferred to the plate is returned to the impactor and the energy gap corresponds to anelastic deformation and damage in the composite.[36] Therefore, these curves permit to show both the role of the damage accumulated and the energy dissipated during the impact.

For the three considered levels of impact energy, the absorbed energy seems to be proportional to the impact energy (Figure 7(a) and (b)). This has often been observed in the case of impact without perforation where the absorbed energy is significantly higher and is usually equal to incoming energy.[41,42] The difference between absorbed energy of $(\pm45)_6$ and $(0/90)_6$ stacking orientation corresponds by 32% and 18% for the impacted energies at 12 and 22J respectively. The shear failure mechanism of +/-45° fibre orientation, as also the anelastic behaviour of the *Elium*® matrix and the flax fibres are two main reasons of that increasing energy.[43] Although the samples with $(\pm45)_6$ stacking orientation has the highest absorbing capacities, the trend to reach the sample perforation for that orientation is 16% higher than for $(0/90)_6$ one (the ratio of Eabs/Eimp corresponds to 87% and 73% at 22J of impact energy for $(\pm45)_6$ and $(0/90)_6$ respectively).

Discussion. Above described impact tests have shown that the $[0/90]_6$ stacking orientation presents better impact resistance than the $(\pm45)_6$ one due to shorter contact time, higher peak force, and less absorbed energy for the impact energy higher than 8J. This trend was also generalized in the literature by several researchers.[41,42,44] However, many studies suggested that adding +/-45° surface layers in the (0/90) composite provides higher resistance to impact and good post-impact compressive strength.[41,45,46] Results show that (0/90/90/0) orientated composite had an opening of inter-layer and more delamination lateral spread which can be avoided using separation of 90 and 0 layer orientation of (90/-45/45/0) composite by -45° and 45° fibre.[42]

To compare the current impact properties of $(0/90)_6$ woven flax/Elium® bio-composite with the literature review, Table 4 presents its overview for similar woven reinforced composites.[7,47–52] Particular attention has been paid to the epoxy matrix reinforced by the flax fibres,[47–49] as it has similar properties to flax/Elium® composite. In addition, the Elium® based composites reinforced by the synthetic woven fabric were also compared to the current bio-composite.[7,50,51]

The overview of results highlights that the current 2/2 twill woven flax/Elium® composite has similar impact properties with epoxy-based composites.[47–49] The peak force of the studied composite is situated in the diapason of epoxy-based one, corresponding to (1.2–3.0) kN for the impact energy of (12–15) J. The average difference is about 5%. Concerning the impact absorbing capacity, the current composite is about 32% tougher than epoxy-based composite at (20–23) impact energies because of the brittle behaviour of the latter. However, the current composite tends faster extend the impact damage. E_{abs}/E_{imp} corresponds to 73% against 30% and 65% for the same diapason of impact energies.

Also, the literature review shows that woven glass and carbon-reinforced Elium® composites are generally twice stiffer than woven flax-reinforced ones. The peak force of

Table 3. Permanent deflection for dry and aged considered bio-composites.

Orientation	Impact energy (J)	Permanent deflection (mm)	
		Dry	Aged
$(0/90)_6$	7.5	1.08	1.50
	12.5	1.38	3.00
	21.4	4.13	7.20
$(\pm45)_6$	8.5	0.75	—
	15.5	2.68	—
	22.77	6.35	—

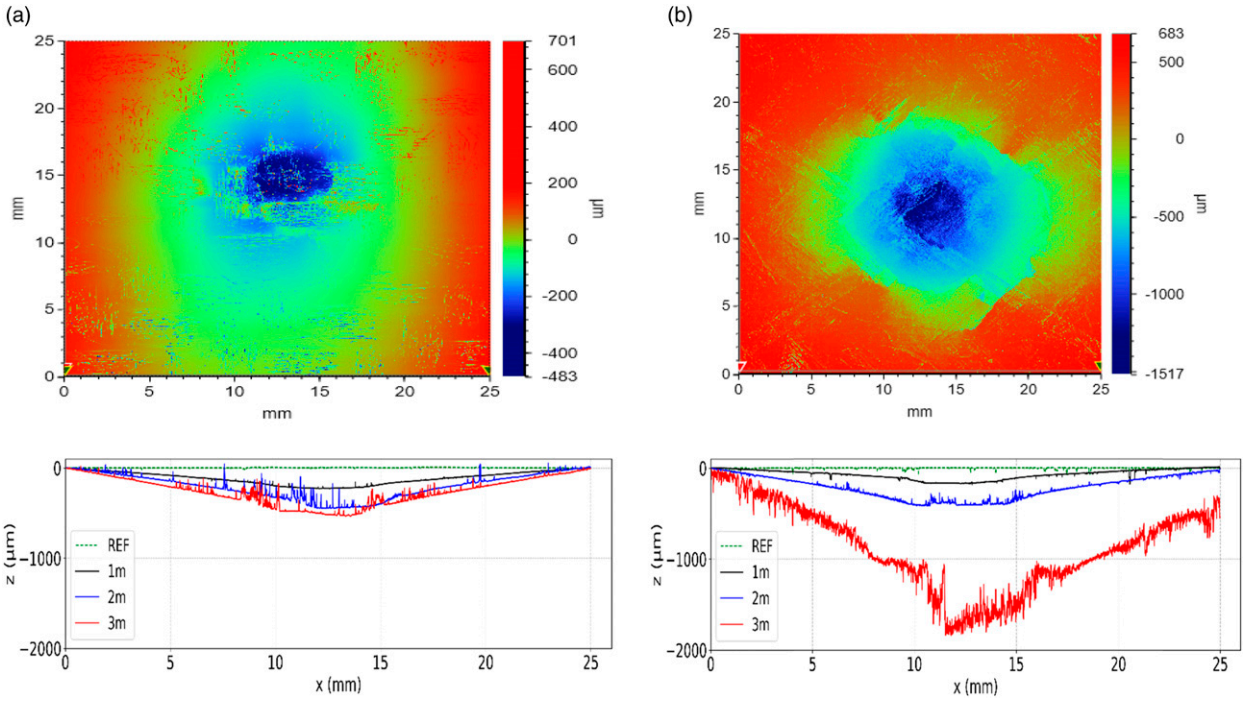

Figure 6. Profilometry scans of surface and indentation depth in the area of 25 × 25 mm^2: (a) $(0/90)_6$. (b) $(\pm45)_6$. The scans represent samples impacted at 22J.

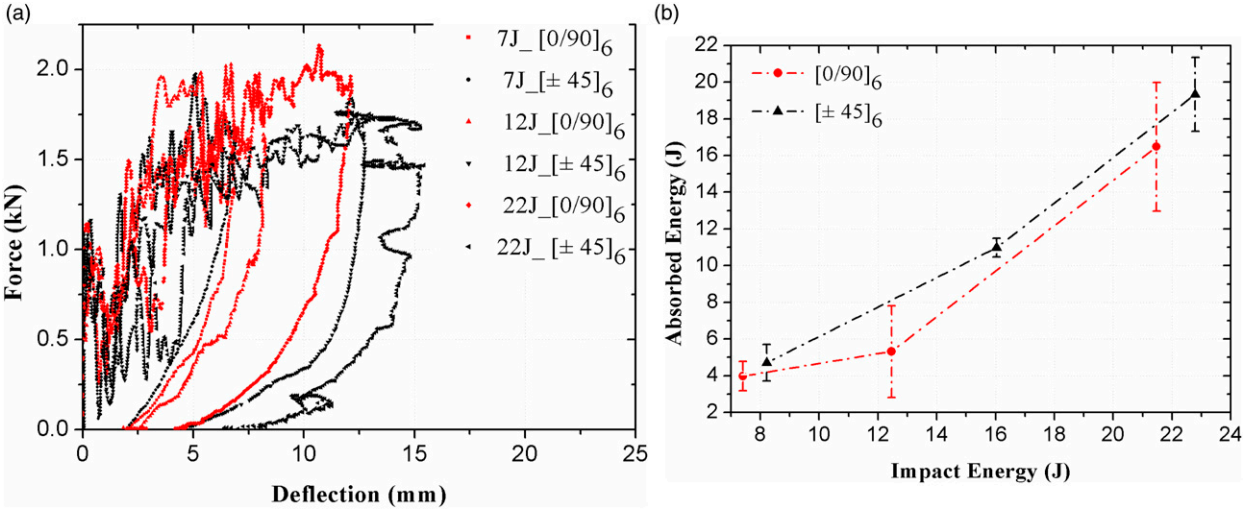

Figure 7. (a) Force vs deflection during impact at 7 J, 12 J and 22 J, (b) absorbed energy comparison.

taffetas and twill woven glass/Elium® composites, as also carbon woven/Elium® composites are 47%, 53%, and 45% respectively higher than twill woven flax/Elium® one at the diapason of impact energy (15J–30J).[7,50,51] In addition, their absorbing capacity is also about twice higher than the current bio-composite. However, woven carbon/Elium® composite tends to perforate 27% faster than considered one due to the brittle behaviour of carbon fibres, while the latter extends 12% faster the impact damage compared to glass fabric reinforcement (see Table 4).

Finally, F. Javanshour et al.[52] have also studied the LVI properties of woven flax/Elium® composite. The authors found similar absorbing capacity, but the peak force was

Table 4. Overview of impact Properties of the woven Reinforced composites.

Composite material	Test condition	Peak force (kN)	Impact energy (J)	Peak deflection (mm)	E_{abs}/e (J/mm)	E_{abs}/E_{imp} (%)	Ref
2/2 twill Woven flax/Epoxy		2.2	6	3.9	0.5	25	[47]
$(0/90)_5$		2.2	12	4.6	1.7	43	
2/2Twill Woven flax/PP		1.9	12	4.1	1.8	47.5	
$[0/90]_{10}$,							
Plate thickness: 3.1 mm± 0.05 mm							
2/2 twill Woven Flax/Epoxy	RT	3	13	5	1.2	54	[48]
$[0/90]_8$		—	23	-	2.5	65	
Plate thickness: 6 mm							
Woven flax/Epoxy $[0/90]_5$	RT	1.2	15	10.54	2.15	36	[49]
Plate thickness: 2.5 mm		1.2	20	16.55	2.4	30	
Woven carbon/Elium® $[0/90]_8$	RT	3.8	15	3.6	8.2	86	[50]
Plate thickness: 1.57 mm							
2/2 twill woven Glass/Elium®	RT	5.7	30	10.9	9.75	65	[7]
$[0/90]_4$		6.7	40	10.8	16.5	82.5	
Plate thickness: 2 mm		6.5	50	11.4	21.3	85.2	
Taffetas woven glass/Elium®	RT	3.1	10	—	3	60	[51]
$[0/90]_4$		4.2	20		6.25	62.5	
Plate thickness: 2 mm							
2/2 twill Woven flax/Elium	Dry	4.67	21	2.84	4.06	100	[52]
$[0/90]_{3S}$	RT	5.29	21	4.13	3.9	93	
Plate thickness: 5 mm	RH	5.46	21	4.58	3.7	88	
2/2 twill Woven flax/Elium®	Dry	1.7±0.2	7	7.5	1.0	60	This
$[0/90]_6$	RH (70°C)	2.0±0.2	12	7.5	1.7	62	work
Plate thickness: 4.5 mm		2.2±0.1	22	13	3.6	73	
		1.75±0.1	22	15	3.9	80	

twice higher compared to the current composite one, subjected to an impact energy of 21J and the same dry environmental conditions. However, their composite showed the perforation damage at that impact energy.

Post-impact damage observations

Visual observations. The post-impact visual observations reveal an indentation mode on the front face due to the compression under impact, and its depth increases with applied impact energy (Figure 8). The orientation of the fibre stacking also affects the shape of damage. For the $(\pm45)_6$ samples, the impacted front face shows deeper indentation than for the $(0/90)_6$ one at an impact energy of 22 J (Figure 8(g) and (h)). The back face of that $(\pm45)_6$ sample exhibits an 'X' pattern damage represented by the shear failure mode where either matrix crack, fibre/matrix debonding, or fibre breakage propagates along the fibre direction orientated at 45° to the bending axis. It is clear that damage (transition from matrix cracking to fibre breakage) extends with increasing impact energy (Figure 8(d)–(h)). The latter is observed locally and affects only the area near the impact, which is also increased with applied impact energy. As for the $(0/90)_6$ samples, a macro-crack is propagated widthwise and is consequently parallel to the direction of the clamping system. The size of the cracking increases with the applied energy level, going from 25 to 45 mm and finally to 95 mm, approaching the width of the plate. At least, Figure 8(i) and (j) summarizes the damage evolution for both considered bio-composites.

High-speed image observations. To complete the previous visual observations and better understand the evolution of plate deflection and damage as a function of impact duration, the high-speed camera was used. The overall mechanism is the following: when the impactor touches the surface of the plate, it first compresses locally the bio-composite that corresponds to moreover, the first peak on the force-time curves (Figure 4(a)–(c)). Therefore, the indentation occurs right at the impact point and forms the crater more or less deeper, depending on the local stiffness of the material, the impact energy, etc. Then, once the maximum local compression has been reached, the plate deforms globally, at which the macroscopic cracks appear (Figure 9).

During the last rebound phase of the impactor, the plate restores the elastic energy to the impactor by pushing it

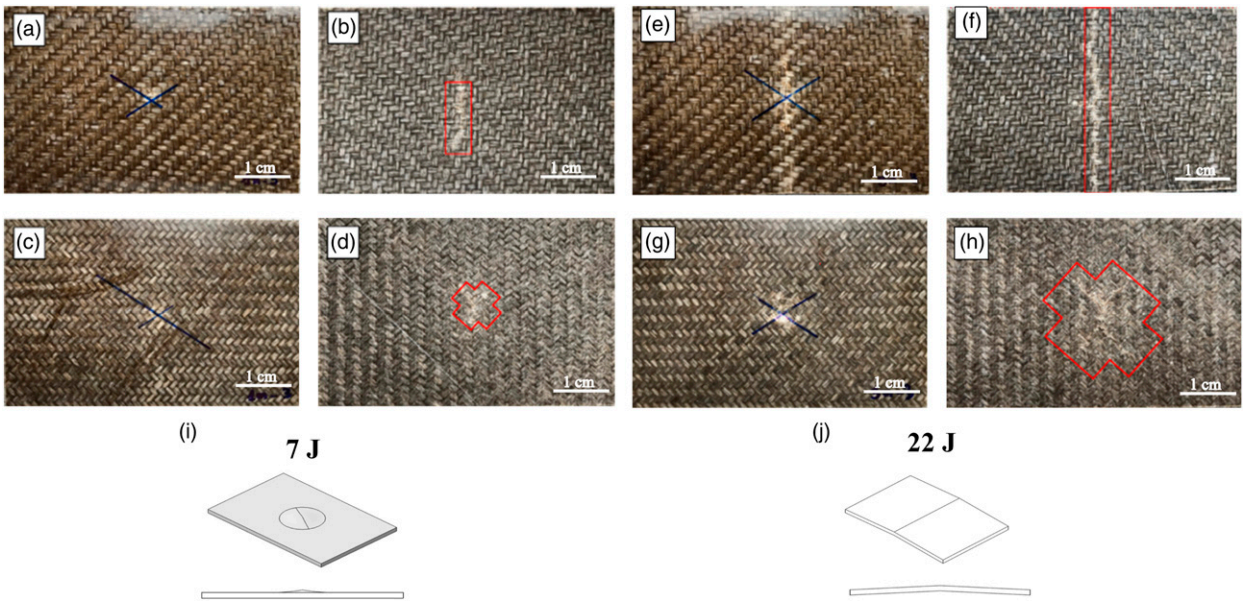

Figure 8. Visual damage evolution after impact from 7 to 22J: (a), (b),(e),(f) - $(0/90)_6$, (c), (d), (g), (h) - $(\pm45)_6$. Left view – top surface and Right view – back surface. *Schema of damage observed for* (i) $(\pm45)_6$ *and* (j) $(0/90)_6$.

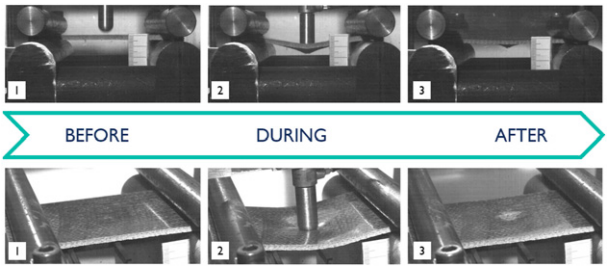

Figure 9. Impact test with high-speed camera: images of deflection evolution captured under two visual angles for the $(\pm45)_6$ flax/Elium® *composite.*

back. The latter, in turn, will show a permanent deflection due to the combined thermoplastic matrix/flax fibre behaviour and visible absorbed damage on its back face. As expected, these phenomena are more and more intense by increasing the impact energy.

Optical microscopic observations. Three different sections of several samples were cut to investigate the damage. The cutting plan is available in Figure 10(a). Area one is the section close to the impact point and parallel to the rod used to clamp the sample (also corresponding to the axis of sample width). Area two is the section perpendicular to the latter and runs along the axis of sample length. Area three is the region far from the impact zone to assume some or no damage due to the impact. As mentioned above, the dry $(0/90)_6$ woven flax/Elium® composite demonstrated better impact performance. It is interesting now to examine in detail its damage progression after impact and determine if it follows the typical conical damage pattern with delamination that is usually observed in unidirectional 0/90° composite laminates.[53] An overview of a cross-section of the observed samples highlights the presence of indentation left by the impactor. The impact indentation is naturally deeper as the impact energy increases by confirming the previous visual observations. The observed damage mechanisms appear mainly in the impacted region of the sample, as area one at 7J and 22J (Figure 10(b) and (d)). The principal damage mechanisms identified for this area are mainly fibre/matrix debonding. Matrix cracking in the form of shear/bending failure was also observed, as well as some delamination due to the stiffness difference of adjacent yarns/layers (mainly developed at 0/90° interfaces), and fibre breakage (due to locally high stresses and indentation effects) with increasing of impact energy. For the energies below 22J, the delamination was few presented (Figure 10(b)). This is due to the resistance to delamination of woven-reinforced composites.[16,41,42] As for the microscopic observations of area two of the $(0/90)_6$ samples, the indentation point was not visible. The principal damage mechanism for this area is also some fibre/matrix debonding (Figure 10(c)). This could be explained by the fact that $[0/90]_6$ samples are damaged in a V-shape and the linear crack propagation is only visible on its widthwise corresponded to the area 1.

In addition, no damage was observed in area 3, which was far from the impacted region (Figure 10(c)). This

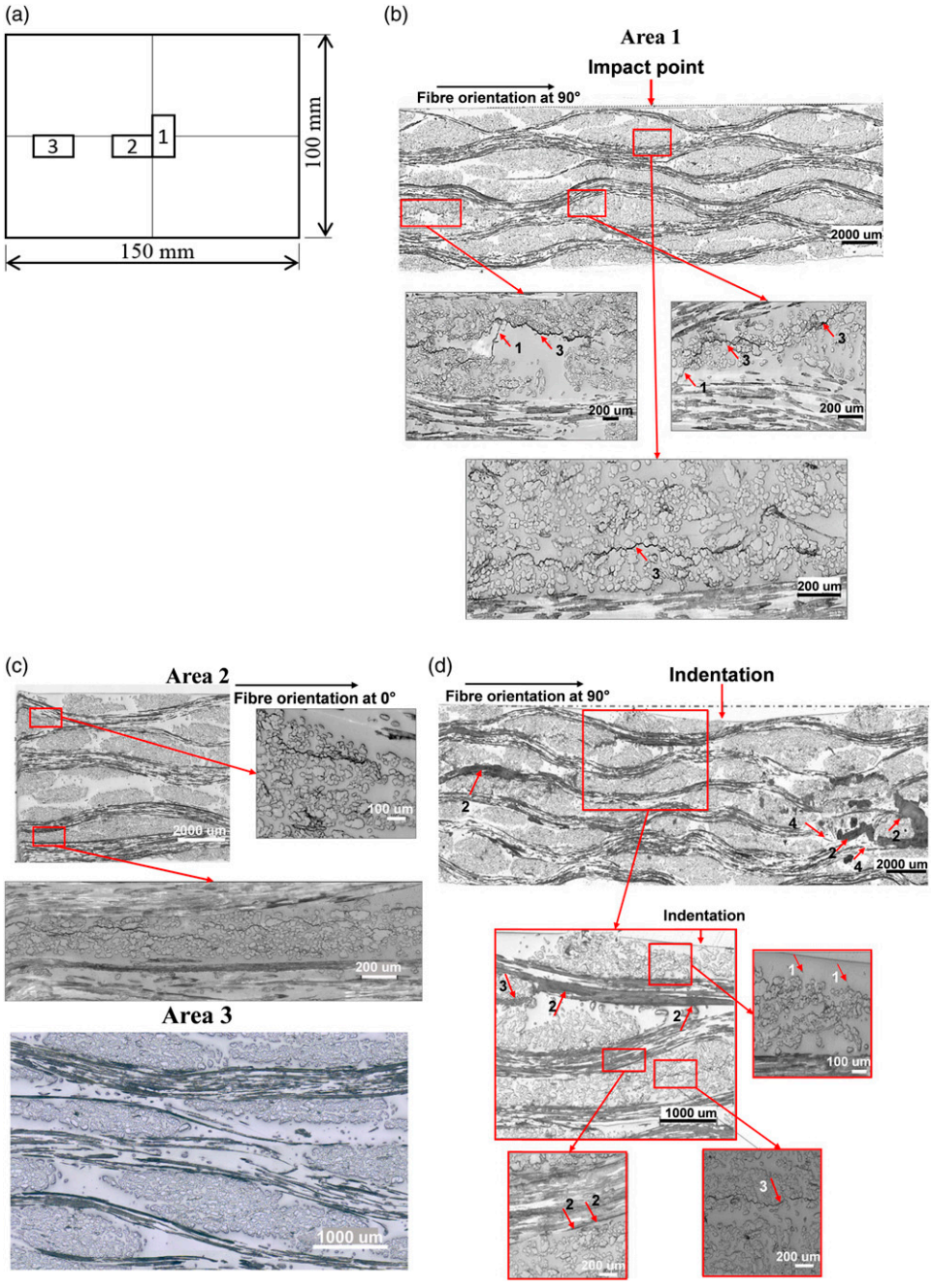

Figure 10. (a) Areas of the plate cut for observation by optical microscope. Microscopic observations of the damages induced by impact at (b) 7J and (d) 22J in the area 1; (c) 22J in the area two and 3. (1) matrix crack propagation, (2) delamination, (3) fibre/matrix debonding; (4) fibre breakage.

proves that the damage after impact is local in the case of woven fibre-reinforced composites.

Post-impact bending

As explained previously, it was considered that bending tests are more suitable than compression ones to study the residual properties after impact. Therefore, the stiffness and the maximum force (for the same considered volume) evolution of the impacted dry $(0/90)_6$ and $(\pm45)_6$ flax/Elium® composites was compared to non-impacted ones considered as the reference. Figure 11 shows the results obtained for both bio-composites. It can be noted that the $(0/90)_6$ orientation has a greater sensitivity to the bending loading than the $(\pm45)_6$ one compared to the reference and between them. Figure 11(a) shows the strong decrease of

residual stiffness and maximum force versus impact damage at 7J–22J for that orientation. Its residual stiffness was 67% and 47% lower regarding the reference and $(\pm45)_6$ orientation respectively subjected to impact energy of 22J. This is expected because the macro-crack observed after impact growths in the widthwise direction of the plate. A linear relation seems to exist between the residual maximum bending force and crack length vs plate width (Figure 11(c)). By contrast, the $(\pm45)_6$ orientation has a similar residual bending behaviour for whatever the impact energy applied. Their residual maximum bending force is about 20% lower than that of the reference (Figure 11(b)). This is probably due to the pattern of the damage because the cracks are diagonally oriented to the bending loading which impact is less evident on the residual bending properties. Better residual tougher behaviour of $(\pm45)_6$ orientation than the $(0/90)_6$ one was also highlighted in the literature.[41,42]

Influence of moisture uptake on the impact response

Figure 12 presents the results of the hygrothermal ageing on the impact properties of the $(0/90)_6$ woven flax/Elium® composite. The force curves of aged samples show a similar overall response, but are smoother than the unaged ones (Figure 12(a)–(c)). It may indicate a softening (reduction in the stiffness) of the sample due to ageing. Decrease of 10, 15, and 20% in the maximum impact load have been observed at 7J, 12J, and 22J impact energies for the aged samples.

The influence of hygrothermal ageing on the permanent and maximum deflection behaviour of the current bio-composite has also been studied with respect to the evolution of impact energies applied (Figure 12(d)). The maximum deflection of aged samples increases by 7%, 34.5%, and 14% at 7J, 12J, and 22J impact energies respectively while the difference in permanent deflection between aged and dry samples is higher 28%, 54%, and 43% respectively (see Table 3). It could be explained by the flax fibres plasticized due to the moisture uptake favorising the high deflection during the impact. The same trend was observed by F.Javanshour[52] for 90% RH of (0/90) woven flax/Elium® composite. However, although the ageing effect is evident in the deflection evolution, no indication of a drastic degradation of impact resistance has been noted. It could be attributed to the Elium® matrix behaviour. It is well known that thermoplastic matrix-based composites offer good ability to conserve their mechanical properties after hygrothermal ageing.[54]

The force vs deflection curve analysis shows better impact resistance of the unaged bio-composite, as already noted for contact force and deflection (Figure 12(e)). A reduction of 40% of the threshold is observed for the aged samples in the same stacking direction (Figure 12(f)). The absorbed energy of the aged samples increases due to the damage accumulation and the plasticization effect of the composite material.

In summary, the aged fibres modified the relative brittle nature of flax- Elium composites through softening due to the plasticising effect of moisture bound to fibres.[55] Indeed, both at humidity levels above 70% RH and high temperature (70°C), water seeps into the fibre and disorganize the microfibrils network, which cause its defibrillation and leads to a decrease of the fibre strength, and therefore, the LVI properties (peak force decrease and increase of max deflection and absorbed energy).[55,56] The decreasing of impact properties under the hydrothermal ageing of the flax reinforced composites has also been reported in the literature.[30,32]

Repair

Thermoplastic matrices are known for their ability to be repaired because they are fusible. Therefore, it is possible to modify or repair the shapes of composite parts, by heating its resin. In the present work, it was assumed that if the low-velocity impact damage does not induce the

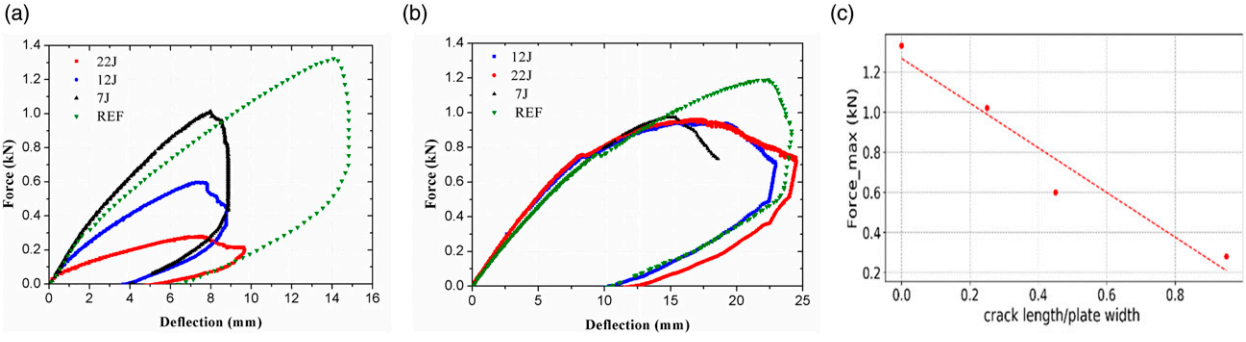

Figure 11. Residual performances after impact for dry (a) $(0/90)_6$ and (b) $(\pm45)_6$ flax/Elium® composites; (c) Relation between the residual maximum bending force vs crack length/plate.

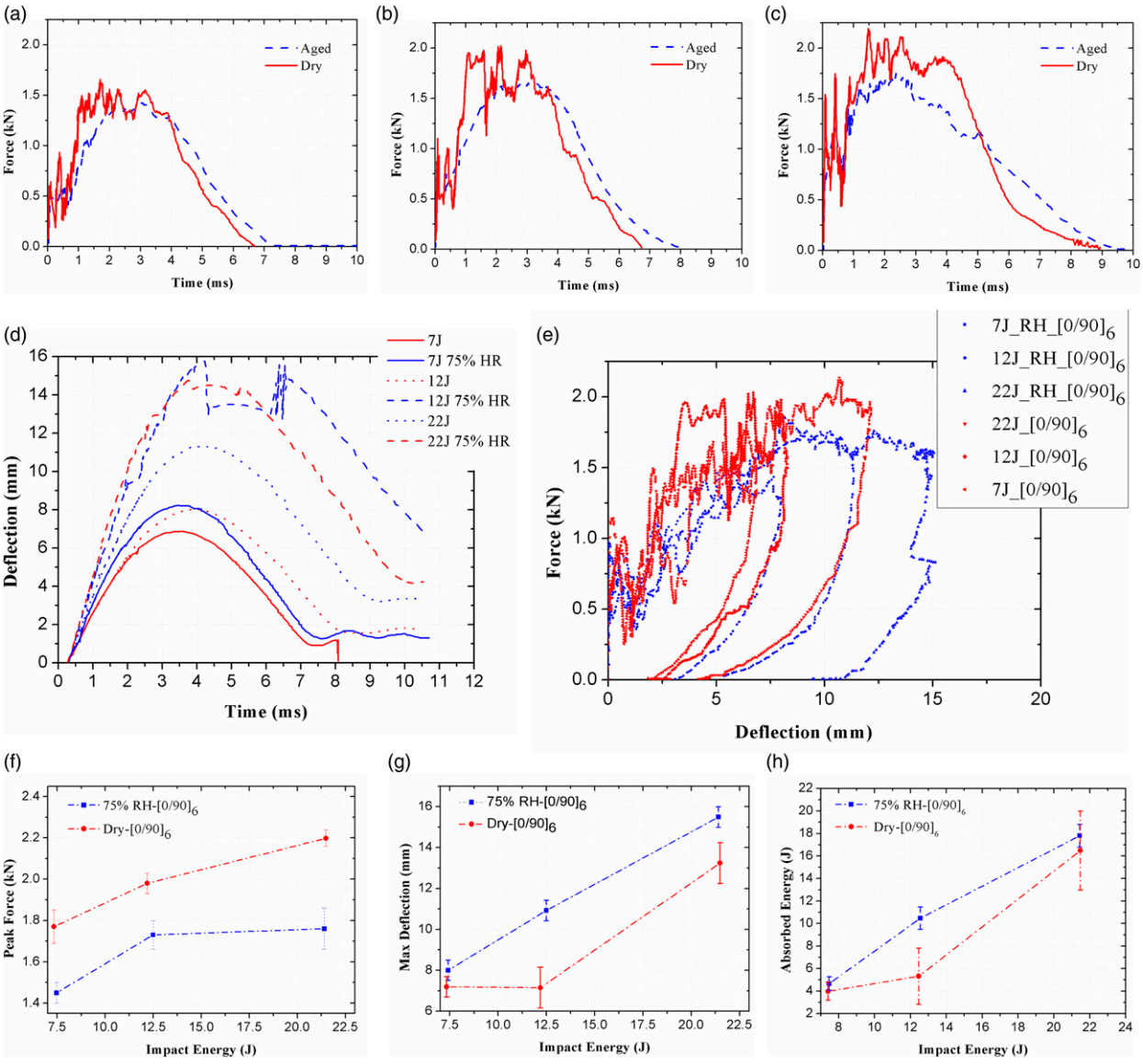

Figure 12. Load versus impact time for around: (a) 7 J, (b) 12 J, (c) 22J; (d) Deflection versus impact time for around 7 J, 12 J and 22J; (e) Force vs deflection during impact at 7 J, 12 J and 22 J; (f) Peak force evolution versus impact energy; (g) max deflection evolution versus impact energy; (h) absorbed energy comparison of dry and 75%RH $(0/90)_6$ orientation.

fibre breakage, the composite parts could be repaired by heating and compressing them again. Two impact energies were chosen for that: the first (7J) induces the fibre breakage, and the second (4J) – none. The $(0/90)_6$ flax/Elium® composite is considered for the repair since its characteristic impact damage on the back face is macro-cracking propagated in the widthwise direction (Figure 4(f)) and, moreover the physical geometry of the plate remains relatively flat that facilities repairing. The repair methodology is following: 1. Impact test conduction; 2. Repair through the thermo-compression cycle described in Manufacturing process; 3. Repete n times the points 1 and 2 to verify residual impact performance. Figure 13(a) shows the load-time curves carried out at 7J of impact energy and correspond to eight impact/repair cycles. The repeated impact events are frequent in the marine and aerospace structures.[41] So, the understanding of their behaviour after repair is primondial. As it could be observed, the maximum impact force (peak force) decreases by about 60%, wherever the contact duration increases by 73% from the 1st to the 8th cycle respectively. It confirms the fact that the impact properties of the plate evolve with each impact/repair cycle applied because of the fibres broken from the first cycle, which strongly

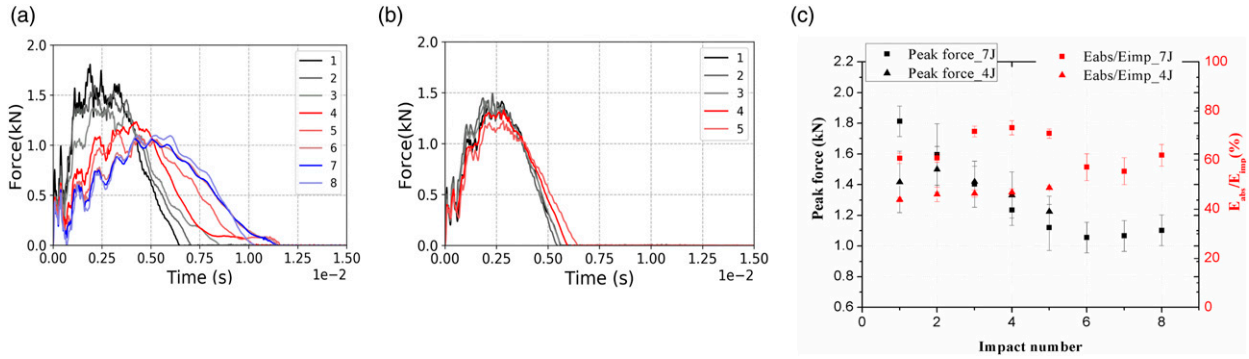

Figure 13. Impact force vs time duration for the multiple impact/repair cycles on $(0/90)_6$ flax/Elium® samples conducted at (a) 7J and (b) 4J; (c) Ratio E_{abs}/E_{imp} and peak force vs the number of impact/repair cycles.

affects the resistance to bending. However, it is possible to see that even with fibre breakage the properties do not change much between two successive curves (Figure 13(a)). Figure 13(b) presents the results of the second (4J) impact energy configuration. Contrary what was observed, the maximum impact force begins to decrease at the 4th impact/repair cycle to reach about 14% of its loss at the 5th cycle. A similar trend was observed for the contact time duration: it increases only by 17% against 73% shown previously. This difference is probably due to the breakage of fibres at an impact energy of 7J, which is irreversible. The results show the great potential of flax/Elium® composite to its repair aptitude. Figure 13(c) compare the peak force and the ratio Eabs/Eimp evolution versus the impact number for both considered impact energies. It confirms the trend of impact peak force evolution observed in Figures 13a and 13(b). In addition, the absorbed energy evolution increases linearly at 4J impact energy and up to 4th cycle at 7J. Note that slope of 4J impact energy is 78% lower than at 7J one due to few damage accumulation at that energy. In contrast, the ratio of E_{abs}/E_{imp} at 7J tends to decrease from 4th to 6th cycle followed by slight increasing for the second time. As the fibre was broken after the first impact, the extend damage continues to progress even after repair cycle up to intensify the maximum of fibre breakage density (associated to decrease of E_{abs}/E_{imp} at 4th – 6th cycles) and tend to reach the perforation damage (the trend of second increase of E_{abs}/E_{imp}) (Figure 13(b)). Additional studies through X-CT tomography analysis are necessary to understand further the effect of multi-impact/repair cycles on the material behaviour of composites.

Conclusion

The present paper focused on the experimental analysis of the low-velocity impact response of woven 2 × 2 twill flax/acrylic thermoplastic resin (Elium®) composites. The effect of impact energy, fibre stacking orientation, moisture uptake, and repair aptitude has been highlighted. Between two considered stacking orientations, the impact resistance was improved for the dry $(0/90)_6$ at impact energies higher than 8J. The main characteristic damage of the current bio-composite is fibre/matrix debonding, sometimes mixed by matrix cracking in the form of shear or bending failure at low impact energies and followed by local delamination and fibre breakage at high impact energy (22J). A correlation between impact energy, damage, and residual properties was established. The $(\pm45)_6$ stacking orientation offers the best residual flexural performance by reducing its maximum flexural force by only 20% at 22J impact energy. Moisture conditioning of $(0/90)_6$ flax/Elium® composite has shown the decrease of 20% in the maximum force, and an increase in the maximum deflection and absorbed energy of 14% and 11% respectively at 22J. The plasticization of flax fibres favors more important deflection and absorbed energy during the impact, by reducing their stiffness. However, no indication of the drastic degradation of impact resistance has been noted. Thermo-compression process was successfully used to repair the impact-damaged $(0/90)_6$ bio-composites. Repetitive impact and repair cycles have shown a significant recovery of stiffness, and maximum impact force up to the 4th cycle at 4J, highlighting the great potential of flax/Elium® bio-composite to its repair aptitude.

Further investigations need to measure the LVI behaviour by FE computations to strengthen the experimental results obtained.

Acknowledgments

The authors would like to thank Gérard Pierre from Arkema for supplying Elium® resin.

Declaration of conflicting interests

The author(s) declared no potential conflicts of interest with respect to the research, authorship, and/or publication of this article.

Funding

The author(s) disclosed receipt of the following financial support for the research, authorship, and/or publication of this article: This work was supported by the Industrial Training and Research Agreement.

ORCID iD

S Terekhina https://orcid.org/0000-0002-4612-0521

References

1. Malkapuram R, Kumar V and Negi YS. Recent development in natural fiber reinforced polypropylene composites. *J Reinf Plast Compos* 2009; 28: 1169–1189. DOI: 10.1177/0731684407087759.
2. Vodicka R. Thermoplastics for airframe applications. A review of the properties and repair methods for thermoplastic composites. Defence Sci and Technol Organisation, DSTO-TR-0424, published by DSTO Aeronautical and Maritime Research Laboratory, Commonwealth of Australia, 1996.
3. Derbali I, Terekhina S, Guillaumat L, et al. Rapid manufacturing of woven comingled flax/polypropylene composite structures. *Int J Mater Form* 2018; 12: 927–942. DOI: 10.1007/s12289-018-01464-1.
4. Campbell F, Jr. *Manufacturing processes for advanced composites*. 1st ed. Amsterdam, Netherlands: Elsevier, 2003, DOI: 10.1016/B978-1-85617-415-2.X5000-X.
5. Zoller A, Escalé P and Gérard P. Pultrusion of bendable continuous fibres reinforced composites with reactive acrylic thermoplastic Elium® resin. *Front Mater* 2019; 6: 290. DOI: 10.3389/fmats.2019.00290.
6. Bhudolia SK, Gohel G, Leong KF, et al. Damping, impact and flexural performance of novel carbon/Elium® thermoplastic tubular composites. *Composites Part B* 2020; 203: 108480. DOI: 10.1016/j.compositesb.2020.108480.
7. Boumbimba RM, Coulibaly M, Khabouchi A, et al. Glass fibres reinforced acrylic thermoplastic resin-based tri-block copolymers composites: Low velocity impact response at various temperatures. *Compos Struct* 2016; 106: 939–951. DOI: 10.1016/j.compstruct.2016.10.127.
8. Richardson MOW and Wisheart MJ. Review of low-velocity impact properties of composite materials. *Compos Part A Appl Sci Manuf* 1996; 27(12): 1123–1131. DOI: 10.11016/1359-835X(96)00074-7.
9. Staszewski WJ, Mahzan S and Traynor R. Health monitoring of aerospace composite structures – Active and passive approach. *Compos Sci Technol* 2009; 69(12): 1678–1685. DOI: 10.1016/j.copscitech.2008.09.034.
10. Atas C and Sayman O. An overall view on impact response of woven fabric composite plates. *Compos Struct* 2008; 82: 336–345.
11. Reyes G and Sharma U. Modeling and damage repair of woven thermoplastic composites subjected to low velocity impact. *Compos Struct* 2010; 92: 523–531. DOI: 10.1016/j.compstruct.2009.08.038.
12. Davoodi MM, Sapuan SM, Ahmad D, et al. Effect of polybutylene terephthalate (PBT) on impact property improvement of hybrid kenaf/glass epoxy composite. *Mater Lett* 2012; 67(1): 5–7. DOI: 10.1016/j.matlet.2011.08.101.
13. Rehman MM, Shaker K and Nawab Y. Effect of poly ether ether ketone particles on v-notched shear and drop weight impact behaviour of carbon/epoxy composite. *Polym Comp* 2022; 43(5): 3219–3227. DOI: 10.1002/pc.26612.
14. Zhang X, Hounslow L and Grassi M. Improvement of low-velocity impact and compression-after-impact performance by z-fibre pinning. *Compos Sci Technol* 2006; 66: 2785–2794.
15. Cantwell WJ and Morton J. The impact resistance of composite materials - a review. *Compos* 1991; 22(5): 347–362. DOI: 10.1016/0010-4361(91)90549-V.
16. Bascom WD, Bitner JL, Moulton RJ, et al. The interlaminar fracture of organic-matrix, woven reinforcement composites. *Compos* 1980; 11(1): 9–18. DOI: 10.1016/0010-4361(80)90016-6.
17. Obande W, Ray D and Ó Brádaigh CM. Viscoelastic and drop-weight impact properties of an acrylic-matrix composite and a conventional thermoset composite – A comparative study. *Mater Lett* 2019; 238: 38–41. DOI: 10.1016/j.matlet.2018.11.137.
18. Bhudolia SK, Perrotey P and Joshi SC. Optimizing polymer infusion process for thin ply textile composites with novel matrix system. *Mater* 2017; 10(3): 293.
19. Bhudolia SK, Perrotey P and Joshi SC. Enhanced Vibration damping and dynamic mechanical characteristics of composites with novel pseudo-thermoset matrix system. *Compos Struct* 2017; 179: 502–513. DOI: 10.1016/j.compstruct.2017.07.093.
20. Bhudolia SK, Perrotey P and Joshi SC. Mode I fracture toughness and fractographic investigation of carbon fibre composites with liquid Methylmethacrylate thermoplastic matrix. *Compos B Eng* 2018; 134: 246–253.
21. Barbosa LCM, Bortoluzzi DB and Ancelotti AC. Analysis of fracture toughness in mode II and fractographic study of composites based on Elium® 150 thermoplastic matrix. *Compos B Eng* 2019; 175: 107082.
22. Bhudolia SK, Joshi SC, Bert A, et al. Flexural characteristics of novel carbon methylmethacrylate composites. *Compos Commun* 2019; 13: 129–133.
23. Kazemi ME, Shanmugam L, Lu D, et al. Mechanical properties and failure modes of hybrid fiber reinforced polymer composites with a novel liquid thermoplastic resin, Elium®. *Compos Part A: Applied Sci and Manuf* 2019; 125: 105523.
24. Bhudolia SK and Joshi SC. Low-velocity impact response of carbon fibre composites with novel liquid Methylmethacrylate thermoplastic matrix. *Compos Struct* 2018; 203(1): 696–708, DOI: 10.1016/j.compstruct.2018.07.066.

25. Faruk O, Bledzki A, Fink H-P, et al. Biocomposites reinforced with natural fibers: 2000–2010. *Prog Polym Sci* 2012; 37: 1552–1596. DOI: 10.1016/j.progpolymsci.2012.04.003.
26. Liang S, Guillaumat L and Gning PB. Impact behaviour of flax/epoxy composite plates. *Int J Impact Eng* 2015; 80: 56–64. DOI: 10.1016/j.ijimpeng.2015.01.006.
27. Corbière-Nicollier T, Gfeller Laban B, Lundquist L, et al. Life cycle assessment of biofibres replacing glass fibres as reinforcement in plastics. *Resour Conserv Recycl* 2001; 33: 267–287. DOI: 10.1016/S0921-3449(01)00089-1.
28. Rowell RM, Young RA and Rowell JK. *Paper and composites from agro-based resources*. London, UK: CRC/Lewis Publishers, 1997.
29. Elium Arkema. *Liquid thermoplastic resin for tougher composites*. Colombes, France: Elium Arkema, 2021. Elium-composites.com
30. Assarar M, Scida D, El Mahi A, et al. Influence of water ageing on mechanical properties and damage events of two reinforced composite materials: Flax-fibres and glass-fibres. *Mater Des* 2011; 32(2): 788–795. DOI: 10.1016/j.matdes.2010.07.024.
31. Li G, Pang SS, Helms JE, et al. Low velocity impact response of GFRP laminates subjected to cycling moistures. *Polym Compos* 2000; 21(5): 686–695. DOI: 10.1002/pc.10222.
32. Živković I, Fragassa C, Pavlović A, et al. Influence of moisture absorption on the impact properties of flax, basalt and hybrid flax/basalt fiber reinforced green composites. *Compos Part B Eng* 2017; 111: 148–164. DOI: 10.1016/j.compositesb.2016.12.018.
33. Baley C. *Fibres naturelles de renfort pour matériaux composites*. Saint-denis, France: Techniques de l'ingénieur, 2013
34. ISO 62:2008. *Plastiques — Détermination de l'absorption d'eau*. Edition 3. Geneva: ISO, 2008.
35. AITM1-0010. *Airbus test method: determination of compression strength after impact*. Blagnac, France: AITM, 2005.
36. David-West OS, Banks WM and Pethrick RA. A study of the effect of strain rate and temperature on the characteristics of quasi-unidirectional natural fibre-reinforced composites. *Proc Inst Mech Eng Part L J Mater Des Appl* 2011; 225(3): 133–148. DOI: 10.1177/0954420711404635.
37. Dhakal HN, Zhang ZY, Richardson MOW, et al. The low velocity impact response of non-woven hemp fibre reinforced unsaturated polyester composites. *Compos Struct* 2007; 81(4): 559–567. DOI: 10.1016/j.compstruct.2006.10.003.
38. Schoeppner GA and Abrate S. Delamination threshold loads for low velocity impact on composite laminates. *Compos Part A Appl Sci Manuf* 2000; 31(9): 903–915. DOI: 10.1016/S1359-835X(00)00061-0.
39. Potluri P, Hogg P, Arshad M, et al. Influence of fibre architecture on impact damage tolerance in 3D woven composites. *Appl Compos Mater* 2012; 19(5): 799–812. DOI: 10.1007/s10443-012-9256-9.
40. Matadi R, Hablot E, Wang K, et al. High strain rate behaviour of renewable biocomposites based on dimer fatty acid polyamides and cellulose fibres. *Compos Sci Technol* 2011; 71(5): 674–682. DOI: 10.1016/j.compscitech.2011.01.010.
41. Shah SZH, Karuppanan S, Megat-Yusoff PSM, et al. Impact resistance and damage tolerance of fiber reinforced composites: a review. *Comp Struct* 2019; 217: 100–121, DOI: 10.1016/j.compstruct.2019.03.021.
42. Kaware K and Kotambkar M. Low velocity impact response and influence of parameters to improve the damage resistance of composite structures/materials: a critical review. *Int J of Crashworth* 2021; 27: 1232–1256. DOI: 10.1080/13588265.2021.1914985.
43. Sarasini F, Tirillò J, Valente M, et al. Hybrid composites based on aramid and basalt woven fabrics: impact damage modes and residual flexural properties. *Mater Des* 2013; 49: 290–302. DOI: 10.1016/j.matdes.2013.01.010.
44. Wu Z, Wu C, Liu Y, et al. Experimental study on the low-velocity impact response of braided composite panel: effect of stacking sequence. *Comp Struct* 2020; 252: 112691. DOI: 10.1016/j.compstruct.2020.112691.
45. Vasudevan A, Senthil Kumaran S, Naresh K, et al. Layer-wise damage prediction in carbon/Kevlar/S-glass/E-glass fibre reinforced epoxy hybrid composites under low-velocity impact loading using advanced 3D computed tomography. *Int J Crashworthiness* 2020; 25: 9–23.
46. Hongkarnjanakul N, Bouvet C and Rivallant S. The effect of stacking sequence on the low-velocity impact response of composite laminates. ECCM15 - 15th European conference on composite materials. Venice, Italy, 24–28 June 2012.
47. Ramakrishnan K-R, Corn S, Le Moigne N, et al. Low velocity impact damage assessment in natural fibre biocomposites. ICCM21 - 21st International Conference on Composite Materials. Xi'an, China, 20–25 August 2017.
48. Cuynet A, Scida D, Roux E, et al. Damage characterisation of flax fibre fabric reinforced epoxy composites during low velocity impacts using high-speed imaging and Stereo Image Correlation. *Comp Struct* 2018; 202: 1186–1194, DOI: 10.1016/j.compstruct.2018.05.090.
49. Wang A, Wang X and Xian G. The influence of stacking sequence on the low-velocity impact response and damping behavior of carbon and flax fabric reinforced hybrid composites. *Polym Test* 2021; 104: 107384. DOI: 10.1016/j.polymertesting.2021.107384.
50. Kazemi ME, Shanmugam L, Dadashi A, et al. Investigating the roles of fiber, resin, and stacking sequence on the low-velocity impact response of novel hybrid thermoplastic composites. *Comp Part B* 2021; 207: 108554. DOI: 10.1016/j.compositesb.2020.108554.
51. Kinvi-Dossou G, Bonfoh N, Matadi Boumbimba R, et al. A mesoscale modelling approach of glass fibre/Elium acrylic woven laminates for low velocity impact simulation. *Comp Struct* 2020; 252: 112671. DOI: 10.1016/j.compstruct.2020.112671.

52. Javanshour F, Prapavesis A, Pournoori N, et al. Impact and fatigue tolerant natural fibre reinforced thermoplastic composites by using non-dry fibres. *Comp: Part A* 2022; 161: 107110. DOI: 10.1016/j.compositesa.2022.107110.
53. Shyr TW and Pan YH. Impact resistance and damage characteristics of composite laminates. *Compos Struct* 2003; 62(2): 193–203. DOI: 10.1016/S0263-8223(03)00114-4.
54. Vieille B, Aucher J and Taleb L. Comparative study on the behavior of woven-ply reinforced thermoplastic or thermosetting laminates under severe environmental conditions. *Mater Des* 2012; 35: 707–719. DOI: 10.1016/j.matdes.2011.10.037.
55. Thuault A, Eve S, Blond D, et al. Effects of the hygrothermal environment on the mechanical properties of flax fibres. *J Compos Mater* 2014; 48(14): 1699–1707. DOI: 10.1177/0021998313490217.
56. Fuentes CA, Ting KW, Dupont-Gillain C, et al. Effect of humidity during manufacturing on the interfacial strength of non pre-dried flax fibre/unsaturated polyester composites. *Compos Part A Appl Sci Manuf* 2016; 84: 209–215.